Springer

Journal of Mechanical Science and Technology 22 (2008) 1561~1567

Journal of Mechanical Science and Technology

www.springerlink.com/content/1738-494x
DOI 10.1007/s12206-008-0318-8

Investigation of gas flow characteristics in proton exchange membrane fuel cell

Lee Ku Kwac and Hong Gun Kim*

Department of Mechanical and Automotive Engineering, Jeonju University, Jeonju, 560-759, Korea

(Manuscript Received January 16, 2007; Revised December 30, 2007; Accepted March 30, 2008)

Abstract

An investigation of electrochemical behavior of PEMFC (proton exchange membrane fuel cell) is performed by using a single-phase two-dimensional finite element analysis. Equations of current balance, mass balance, and momentum balance are implemented to simulate the behavior of PEMFC. The analysis results for the co-flow and counter-flow mode of gas flow direction are examined in detail in order to compare how the gas flow direction affects quantitatively. The characteristics of internal properties, such as gas velocity distribution, mass fraction of the reactants, fraction of water and current density distribution in PEMFC are illustrated in the electrode and GDL (gas diffusion layer). It is found that the dry reactant gases can be well internally humidified and maintain high performance in the case of the counter-flow mode without external humidification while it is not advantageous for highly humidified or saturated reactant gases. It is also found that the co-flow mode improves the current density distribution with humidified normal condition compared to the counter-flow mode.

Keywords: PEMFC; Electrodes; Membrane; Gas diffusion layer; Current density; Electric potential; Mass fraction

1. Introduction

Fuel cells are electrochemical devices that convert the chemical energy of a hydrogen based gaseous fuel and oxygen gas or air into electrical energy to drive an external load. Currently, PEMFCs are the most promising type of fuel cells given their potential to replace existing internal combustion engines in automotive applications. During the past decade, many researchers' attention has been devoted to the development of KW scale applications on the electric vehicles driven by fuel cell, which results in most of the world's major automobile industries racing to develop fuel cell passenger vehicles [1]. On the other hand, small fuel cells, which can replace the traditional batteries in such portable electronic devices as mobile phones, laptop, palmtop and solar hydrogen systems [2-6], have been received increasing interest. Among many kinds of fuel cells, the PEMFC is usually regarded as the most promising fuel cell type for the applications.

Compared to typical batteries, fuel cells have characteristics similar to them but differ in several respects. For example, a battery is an energy storage device, with the maximum available energy determined by the amount of chemical reactant stored in the battery; while the fuel cell is a device which converts chemical energy directly into electrical energy and stands for longer operating times and fast refueling, when compared with the traditional battery. At the same time fuel cells are more sensitive to impurities in fuel and air compared to a traditional battery. In addition, the environmental effect of discarded batteries is regarded as a problem, but the waste products of fuel-cell reactions are water and heat. Unfortunately, fuel cell technology is not mature enough to compete with established battery technologies [7]. The cost of fuel cells still remains high and it is not affordable for most consumers, and very few

*Corresponding author. Tel.: +82 63 220 2613, Fax.: +82 63 220 2959
E-mail address: hkim@jj.ac.kr

products are available with full commercial warranties and a track record for reliable operation. Other barriers to commercial use are as follows: fuel cell cost, fuel cell durability, fuel infrastructure, and hydrogen storage. As to the PEMFC, thermal and water management is important [8-11], because PEMFC is operated and effected at relatively low temperature [12], around 330-350 K, and requires humidification of the air and fuel supplies to prevent performance degradation.

The objective of this paper is to model and simulate PEMFCs in order to analyze the fuel cell performance in the case of different gas flow directions. Given that PEMFCs are relatively expensive to produce, numerical modeling and computer simulation have proved to be effective tools in optimizing their efficiency before investing resources into physically doing so. The characteristics of internal properties in PEMFC are presented in detail to investigate the steady state behavior in the electrode and GDL (gas diffusion layer). Finally, the co-flow and counter-flow mode behavior is examined to compare quantitatively. The discrepancy of different flow direction shows no significant effects on the performance of PEMFCs, which gives an insight for the design of PEMFCs.

2. Analysis

The three-dimensional geometry of the cell for PEMFC model is simplified by treating only a two-dimensional cross section as indicated in Fig. 1. It is composed of three domains−anode, proton exchange membrane, and cathode−and each of the porous electrodes is in contact with an interdigitated gas distributor, which has an inlet channel, a current collector, and an outlet channel. Hydrogen is fed into the channel of the anode, and at the same time, humidified air is fed into the cathode. At the anode, hydrogen reacts and is consumed in the active layer to form protons that carry the ionic current to the cathode, while at the cathode, oxygen reacts with protons to form water, at the active layer as in the following way:

$$H_2 \rightarrow 2H^+ + 2e^- \quad \text{at the anode} \tag{1}$$

$$O_2 + 4H^+ + 4e^- \rightarrow 2H_2O \quad \text{at the cathode} \tag{2}$$

In order to simulate the behavior of PEMFC, current balance, mass balance, and momentum balance are implemented with the COMSOL Multiphysics program [13] in this model. The potential distribution

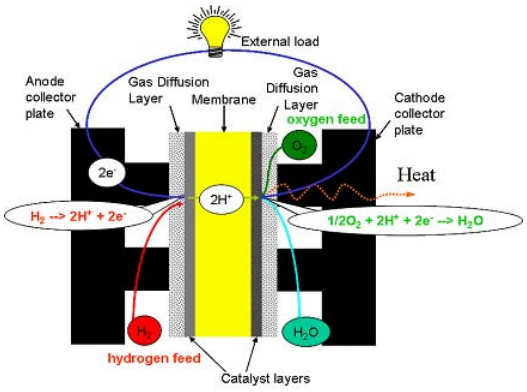

Fig. 1. Schematic of the PEMFC working principle.

is modeled in three subdomains, which are given by following equations.

$$\nabla \cdot (-k^{s,eff} \nabla \phi_s) = 0 \quad \text{at Anode} \tag{3}$$

$$\nabla \cdot (-k^{m,eff} \nabla \phi_m) = 0 \quad \text{at Membrane} \tag{4}$$

$$\nabla \cdot (-k^{s,eff} \nabla \phi_s) = 0 \quad \text{at Cathode} \tag{5}$$

where $k^{m,eff}$ is an effective conductivity (S/m) which is generally a function of relative humidity. However, it is fixed as the value of 9 S/m assuming at 100 % relative humidity condition to investigate the general physical phenomena. The potential (V) at the electrode phases is denoted by ϕ_s, while in the membrane it is denoted by ϕ_m. Within the electrode pores, the gas-phase is considered as a continuous phase and, thus, its momentum conservation equation can be represented by Darcy's law [14].

$$u = -\frac{k_p}{\eta} \nabla p \tag{6}$$

where, k_p denotes the permeability (m^2) of the electrode, η denotes the viscosity (kg/m/s) of the gas and p denotes the pressure (Pa).

Maxwell-Stefan diffusion and convention equation is used in anode and cathode respectively, for the former H_2 and H_2O are considered; for the latter, the O_2, H_2O, and N_2 are considered.

$$\frac{\partial}{\partial_t} \rho \omega_i + \nabla \left[-\rho \omega_i \sum_{j=1}^{N} D_{ij} A + \omega_i \rho u + D_i^T \frac{\nabla T}{T} \right] = R_i \tag{7}$$

Hence, A depicts a function of mass fraction, mole

mass and pressure as below.

$$A=\left\{\frac{M}{M_j}\left(\nabla\omega_j+\omega_j\frac{\nabla M}{M}\right)+\left(x_j-\omega_j\right)\frac{\nabla p}{p}\right\} \tag{8}$$

where T is the temperature (K), $\boldsymbol{u}$ is the velocity (m·s^{-1}) of fluids, $\boldsymbol{x}$ is mole fraction, $\boldsymbol{w}$ is mass fraction, $\mathbf{M}$ is the mole masses (kg·mol^{-1}), D_{ij} is the diffusion coefficient (m^2·s^{-1}), D_i^T is the transpose of the diffusion coefficient matrix, R_j is the velocity of reacting matters, p denotes the pressure (Pa), and ρ is the density (kg·m^{-3}), which is given by the equation below.

$$\rho=\sum_i x_i M_i \tag{9}$$

Boundary conditions are specified here based on the linear physical properties. The upper and bottom line assumed to be left insulated. The boundary condition of the current density at the interface between the anode and the membrane can be imposed as the previous study [14]. Hence, it is imposed as the active layer thickness with the value of 1.0×10^{-5} m, the agglomerate particle radius with the value of 1.0×10^{-7} m, the Faraday's constant with the value of 96,487 A·s/mol, the universal gas constant with the value of 8.314 J/mol·K, the fixed temperature with the value of 353 K, the potential at the anode current collector with the value of $0V$. In the same fashion, the dry porosity of electrodes with the value of 0.4, the specific surface area of the electrodes with the value of 1.0×10^7 m^2, the gas viscosity in the electrode pores with the value of 2.1×10^{-5} (Pa·sec). Likewise, the boundary condition of the current density at the interface between the cathode and the membrane can be imposed as the previous study [14].

Concentration of the dissolved hydrogen and oxygen at the surface of the agglomerate particles is defined by the Henry's law, which is given by the equation below.

$$C_{H_2}^{agg}=p_{H_2}y_{H_2}/H_{H_2} \tag{10}$$

$$C_{O_2}^{agg}=p_{O_2}y_{O_2}/H_{O_2} \tag{11}$$

where $C_{H_2}^{agg}$ is the agglomerate hydrogen concentration in the active layer, $y_{H_2,in}$ is molar fraction of hydrogen at the anode inlet with the value of 0.6, $C_{O_2}^{agg}$ is the agglomerate oxygen concentration in the active layer, $y_{O_2,in}$ is molar fraction of oxygen at the cathode inlet with the value of 0.21. On the other hand, H_{H_2} is Henry's concentration coefficient for hydrogen with the value of 3.9×10^4 (Pa·m^3/mole), and H_{O_2} is Henry's concentration coefficient for oxygen with the value of 3.2×10^4 (Pa·m^3/mole). The current density, normal to the membrane domain, which is at the interfaces between the electrodes and the membrane, can be written by:

$$(-k^{m,eff}\nabla\phi_m)\cdot n=-i_a \quad \textit{at the boundary between anode and membrane} \tag{12}$$

$$(-k^{m,eff}\nabla\phi_m)\cdot n=-i_c \quad \textit{at the boundary between membrane and cathode} \tag{13}$$

The mass transfer of species across the anodic and cathodic active layers is also related to the local current density according to:

$$-n\cdot n_{H_2}=-\frac{i_a}{2F} \quad \textit{at the anodic active layer} \tag{14}$$

$$-n\cdot n_{O_2}=\frac{i_c}{4F} \quad \textit{at the cathodic active layer} \tag{15}$$

$$-n\cdot n_{H_2O}=d_{H_2O}\frac{i_c}{2F} \quad \textit{at the cathodic active layer} \tag{16}$$

where d_{H_2O} is the drag factor of water. Assuming that hydrogen proton carries water particle of three, so the value of 3 is implemented as d_{H_2O}. At the remaining boundaries it is applied to insulated or symmetric conditions. The potential at the anode current collector is set as $\phi_s=0$, and cathode is set as $\phi_s=V_{cell}$, where V_{cell} is the potential at the cathode current collector, with the value of 0.6 V. The gas pressure of the inlet is used as 1.1 times of atmospheric pressure and that of outlet is set as atmospheric pressure.

3. Modeling

The PEMFC model is based on the real geometry and is presented here as shown in Fig. 2. The model is a unit cell with appropriate boundary conditions repeating through the channel. Here, electrode height is 2mm, electrode width is 0.25mm, membrane thickness is 0.1mm, and current collector height is 1mm, respectively. Fig. 2 shows the repeated unit cell model describing gas flow direction. Fig. 3 shows finite element meshes generated under the boundary condition as described above. The mesh size is con-

trolled in the most refined manner in the vicinity of the current collector ends.

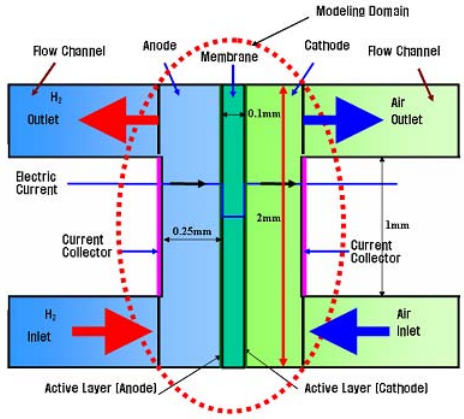

(a) Co-flow mode

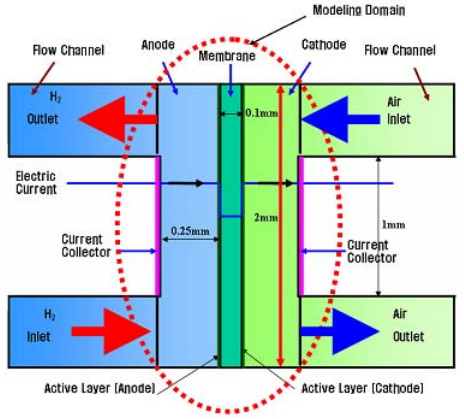

(b) Counter-flow mode

Fig. 2. The repeated unit cell model of PEMFC showing gas flow direction.

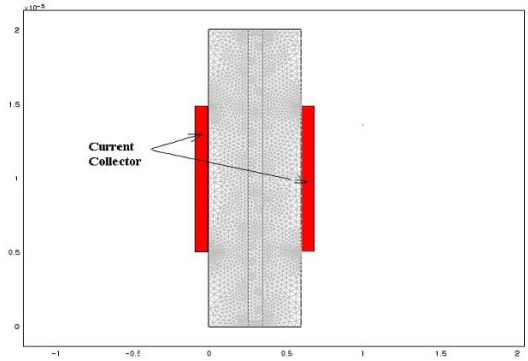

Fig. 3. The generated finite element mesh of the model.

4. Results and discussion

Fig. 4 compares the calculated fuel cell potential as a function of current density with experimental data. The fuel cell is operated with humidified gases in the counter flow mode. It can be found that modeling results compare well with the experimental results. Nafion 115 membrane is used in this test. The simulation results on the gas flow direction are described from Figs. 5 through 9 with the humidified normal condition. Fig. 5 shows the velocity distribution in association with hydrogen and air at the anode and cathode, respectively. The even velocity distribution along the active layer indicates that strong convective flux occurs in the GDL. Fig. 5 also shows that the discrepancy of gas velocity for the co-flow and counter-flow mode points out little difference of the effects on opposite gas flow directions. Fig. 6 shows the reactant mass fraction, which is normalized by its inlet value. The hydrogen mass fraction increases along the electrode from the inlet to the outlet, which means the drag induced flux of water is higher than the hydrogen consumption; while, in the cathode the oxygen mass fraction varies little because of the stoichiometric excess in the inlet of the cathode for the both of co-flow and counter-flow modes.

On the other hand, the water management is extremely important in the performance of PEMFCs. Hence the water mass fraction is investigated in detail. Fig. 7 shows the water mass fraction in the anode and cathode gases as well as the diffusive flux of water in the case of co-flow and counter-flow mode. It is apparent that water is transported through both diffusion and convection to the membrane on the anode side. This decreasing water content results in a minimum

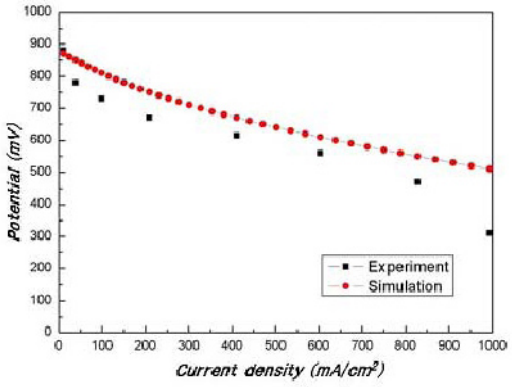

Fig. 4. Comparison of the simulation result and experiment data for humidified normal cases.

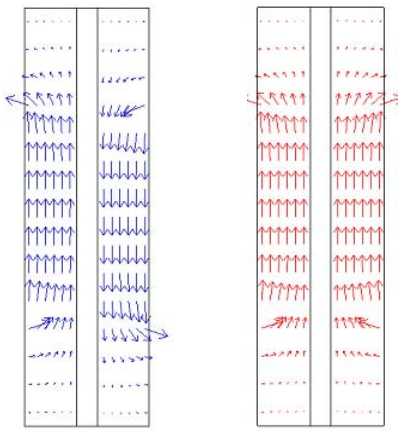

(a) Co-flow mode (b) Counter-flow mode

Fig. 5. Normalized gas velocity fields for the co-flow and counter-flow mode for humidified normal cases.

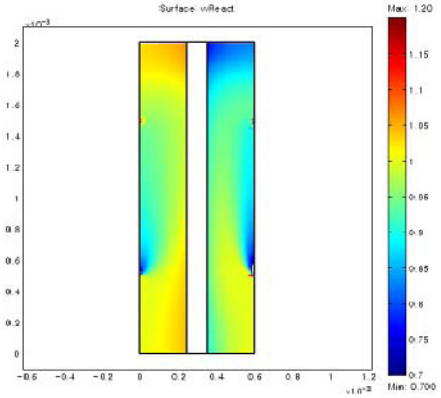

(a) Co-flow mode

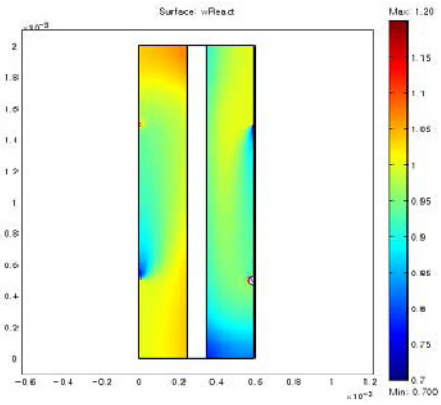

(b) Counter-flow mode

Fig. 6. Reactant mass fraction normalized by its inlet value for the co-flow and counter-flow mode for humidified normal cases.

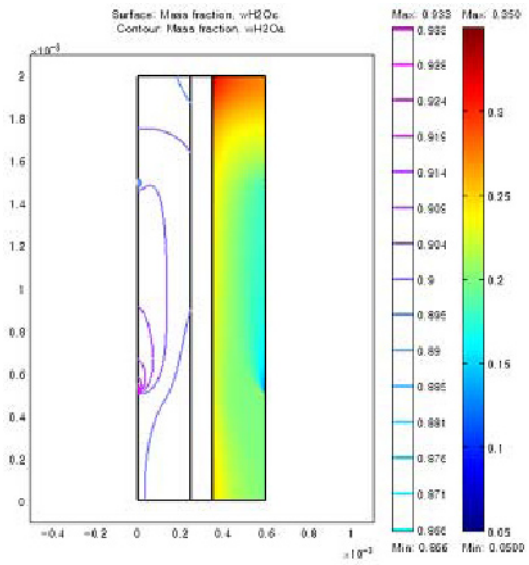

(a) Co-flow mode

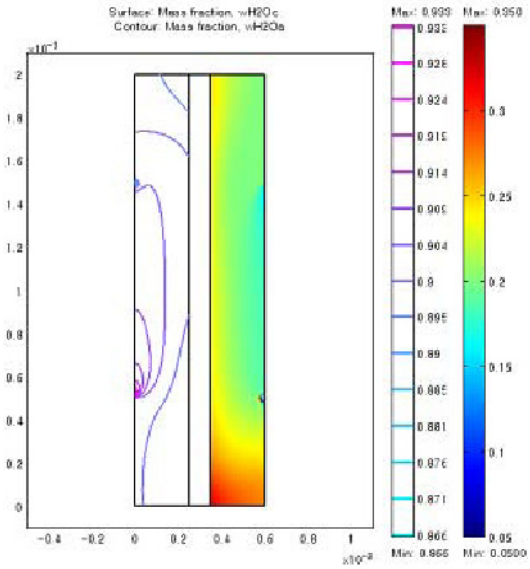

(b) Counter-flow mode

Fig. 7. Fraction of water in the anode (left) and cathode (right) the co-flow and counter-flow mode for humidified normal cases.

occurring in the upper corner of the membrane at the anode. This is known to limit the performance of fuel cells as, if the gas becomes too dry, the membrane dries out and subsequently fails. However, at cathode, water levels increase with the direction of flow and a local maximum in water current occurs in the upper

corner of the membrane for the co-flow mode and in the lower corner of the membrane for the counter-flow mode. This may also be critical in that water droplets may clog the pores and effectively hinder gas transports to the active layer.

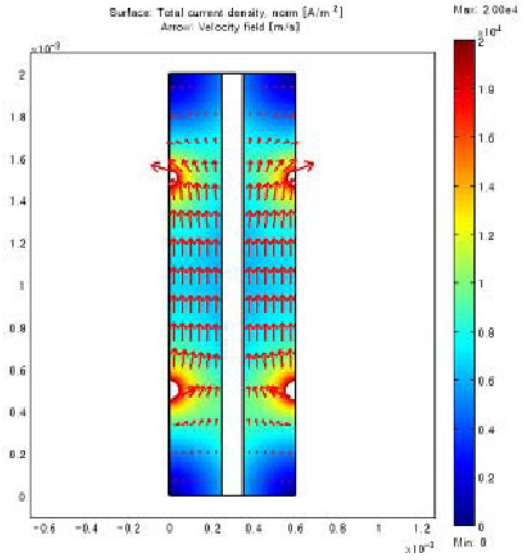

(a) Co-flow mode

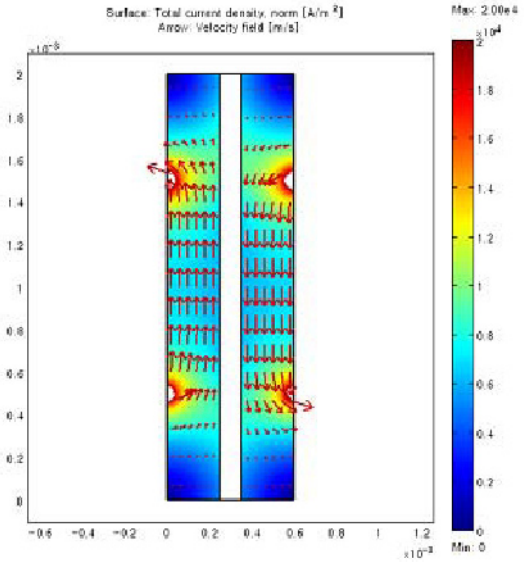

(b) Counter-flow mode

Fig. 8. Current density distribution in the fuel cell operating at 0.6 *V*. The anode and cathode is on the left and right, respectively. Arrows depict the current flux showing the direction and magnitude.

Fig. 8 shows the current density distribution in the fuel cell operating at 0.6*V*. The current density increases from the center to the edges of the current collectors and this results from the variation of flowing hydrogen velocity along the gas channel. It is also shown that the current density distribution of the co-flow and counter-flow mode indicates no significant change for the gas flow direction for humidified normal cases.

Fig. 9 shows that the current density at the active layer is plotted as a function of fuel cell height (y-axis). The current density is different according to the arc-length: the highest current density is presented in the lower region of the PEMFC for the co-flow mode as can be seen in Fig. 9 (a), while it is presented in the upper region for the counter-flow mode as can be seen in Fig. 9 (b). This means the current density is heavily dependent on the oxygen reduction reaction rate in the cathode as well as not affected significantly by gas flow direction in the cathode for the humidi

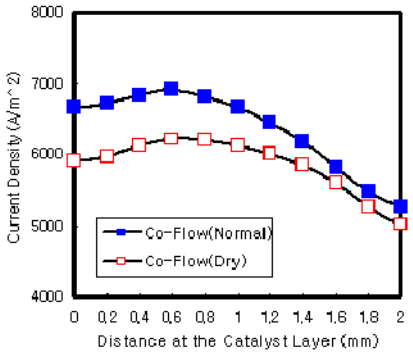

(a) Co-flow mode

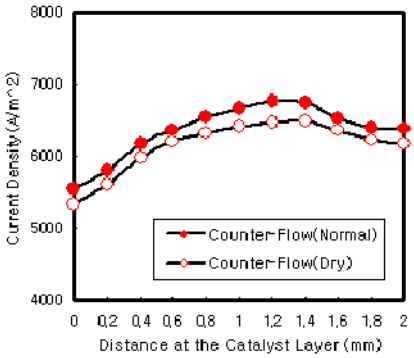

(b) Counter-flow mode

Fig. 9: The current density at the active layer for the normal and dry condition. Units of current density and arc-length are A/m^2 and *mm*, respectively.

fied normal condition. However, it is found that the dry reactant gases can be well internally humidified and maintain high performance in the case of the counter-flow mode without external humidification while it is not advantageous for highly humidified or saturated reactant gases. It is also found that the co-flow mode improves the current density distribution with humidified normal condition compared to the counter-flow mode.

5. Conclusions

A single phase PEMFC model has been studied to investigate the effects on the gas flow direction. The model takes into account two-dimensional flow of momentum, current and mass on the cathode side, as well as conservation of charge throughout the whole cell repeated. Special attention is given to ensure that the model is simulated under conditions similar to the real PEMFC. The co-flow and counter-flow mode behaviors concerning the gas flow direction are examined to compare quantitatively. It is found that the discrepancy of different flow direction gives no significant effects on the performance of PEMFCs for the humidified normal condition. However, it is found that the dry reactant gases can be well internally humidified and maintain high performance in the case of the counter-flow mode without external humidification while it is not advantageous for highly humidified or saturated reactant gases. It is also found that the maximum current density at a constant cell voltage occurs at the center to outlet region of the cell in the active layer of the electrode.

References

[1] C. Marr and X. Li, Two-dimensional finite element method study of the resistance of membranes in polymer electrolyte fuel cells, *Electrochimica Acta*, 45 (2000) 1741-1751.

[2] D. M. Bernardi and M. W. Verbrugge, Mathematical model of a gas diffusion electrode bonded to a polymer electrolyte, *AIChe Journal*, 37 (1991) 1151-1163.

[3] C. K. Dyer, Fuel Cells for Portable Applications, *Journal of Power Sources*, 106 (2002) 31-34.

[4] J. P. Meyers and H. L. Maynard, Design considerations for miniaturized PEM fuel cells, *Journal of Power Sources*, 109 (2002) 76-88.

[5] J. W. Raadschelders and T. Jansen, Energy sources for the future dismounted soldier: the total integration of the energy consumption within the soldier system, *Journal of Power Sources*, 96 (2001) 160-166.

[6] C. Heinzel et al., Fuel cells for low power applications, *Journal of Power Sources*, 2 (105) (2002) 250-255.

[7] W. C. Yang, Fuel cell electric vehicle: Recent advances and challenges, *International Journal of Automotive Technology*, 1 (1) (2000) 9-16.

[8] T. F. Fuller and J. Newman, Water and thermal management in solid-polymer-electrolyte fuel cells, *Journal of Electrochemical Society*, 140 (1993) 1218-1226.

[9] J. S. Yi and T. V. Nguyen, An along the channel model for PEMFC, *Journal of Electrochemical Society*, 145 (1998) 1149-1156.

[10] J. S. Yi and T. V. Nguyen, Multi-component transport in porous electrodes in proton exchange membrane fuel cells using the interdigitated gas distributors, *Journal of Electrochemical Society*, 146 (1999) 38-45.

[11] He, W. et al., Two-phase flow model of the cathode of pem fuel cells using interdigitated flow field, *AIChe Journal*., 46 (2000) 2053-2059.

[12] H. G. Kim, et al., Electric voltage and current characteristics of fuel cell for machine tool power supply, *Journal of Korean Society for Machine Tool Engineers*, 14 (2005) 1-7.

[13] COMSOL AB, Comsol Multiphysics Manual Ver. 3.3 : The proton exchange membrane fuel cell, Burlington, MA, USA, (2006).

[14] H. S. Fogler, Element of Chemical Reaction Engineering, Third Ed., Prentice Hall, (1999).